Shaping of single-cycle sub-50-attosecond pulses with multilayer mirrors

Charles Bourassin-Bouchet, Sébastien de Rossi, Jihuan Wang, Evgueni Meltchakov, Angelo Giglia, Nicola Mahne, Stefano Nannarone, Franck Delmotte

Shaping of single-cycle sub-50 attosecond pulses with multilayer mirrors

C. Bourassin-Bouchet[1], S. de Rossi[1], J. Wang[1], E. Meltchakov[1], A. Giglia[2], N. Mahne[2], S. Nannarone[2] and F. Delmotte[1]

[1]Laboratoire Charles Fabry, UMR 8501, Institut d'Optique, CNRS, Univ Paris Sud 11, 2, Avenue Augustin Fresnel, 91127 Palaiseau Cedex, France

[2]Istituto Officina dei Materiali-Consiglio Nazionale delle Ricerche Laboratorio Tecnologie, Avanzate e NanoSCienza, Area Science Park Basovizza, S.S. 14 Km 163.5, 34149 Trieste, Italy

E-mail: sebastien.derossi@institutoptique.fr

Abstract. We report on the study of multilayer mirrors designed to compress extreme-ultraviolet pulses below 50 as. The mirrors were optimized in the time-domain to get the wanted pulse shape and duration when combined with a broadband hybrid filter. Moreover they appeared to be very robust to environmental parameters, ensuring a pulse compression in various conditions. We manufactured the mirrors and characterized them on a synchrotron facility both in amplitude and phase. The measurement of the latter was performed using the photocurrent technique, which is the only method allowing one to access to the mirrors absolute spectral phase. This led to a measurement of the offset induced by the mirrors on the carrier-envelope phase of attosecond pulses.

PACS numbers: 42.65.Re 42.65.Ky 07.85.Fv

1. Introduction

The perfect synchronization of a broadband emission in the extreme ultraviolet (XUV) range is the key to generate ultrashort pulses at the attosecond time scale. Such a radiation can nowadays be produced thanks to a process named high order harmonic generation (HHG) [1, 2], resulting from the nonlinear interaction of an infrared (IR) femtosecond field with a gaseous [3, 4] or solid target [5]. However, the spectral components of such attosecond pulses were proved to be linearly desynchronized [6], due to a positive group delay dispersion (GDD). This phenomenon commonly called the atto-chirp is intrinsic to HHG, and inevitably broadens pulses. To compensate for this temporal chirp, it has been proposed either to optimize the HHG conditions [7], or to add on the way an optical component inspired by what already existed for visible or IR femtosecond pulses. Such a post-compression can be perform thanks to chirp multilayer mirrors [8, 9, 10, 11], grating compressors [12], or the natural dispersion of metallic filters [13] or gaseous media [14]. Some of these solutions have been successfully implemented

experimentally and allowed one to get isolated 80 as pulses [15] and trains of 63 as pulses [14]. The phenomenon preventing from obtaining even shorter pulses appears to be the width of the spectral range on which the chirp compensation is performed.

However, in the case of visible femtosecond pulses, a solution called the time-domain optimization, has been developed to control the synchronization of a broadband radiation using chirped multilayer mirrors. Indeed, instead of targeting a wanted spectral behaviour, *i. e.* a wanted GDD, during the design of the multilayer structure, one directly optimizes the temporal profile of the reflected pulse. This improves the compression efficiency of the mirrors, which allowed one to get single-cycle sub-5 fs pulses [16, 17]. It was proposed to transpose this approach into the XUV domain [18] to get 100 as pulses.

In this article, we report on the theoretical and experimental study of time domain optimized multilayer mirrors to obtain sub-50 as pulses. To reach such a short duration, the dispersion has to be controlled over a spectral range larger than 100 eV. This bandwidth is isolated from the rest of the spectrum by an aluminum-beryllium filter. Then the resulting pulse is shaped by the optimized multilayer mirror. We confirmed the robustness of the pulse profiles for reasonable experimental conditions. We then fabricated and characterized the mirrors in amplitude and in phase on synchrotron radiation. The spectral phases of the mirrors were reconstructed over a 120 eV bandwidth using the total electron yield standing wave method [19]. Finally, we deduced the attosecond reflected electric field from these measurements.

2. Conditions for the optimization

2.1. The attosecond source

In order to design a multilayer mirror suitable for realistic conditions, we chose typical generation parameters for the simulations of the spectrum $S_{source}(\omega)$ and the spectral phase $\varphi_{source}(\omega)$ of the attosecond source. To be more specific, the wavelength of the driving femtosecond laser pulse equals 800 nm, and its intensity I_{IR} is chosen to be $5.8 \times 10^{14}\, W.cm^{-2}$, which is a typical value [6, 14, 15]. The XUV radiation is generated in neon. Moreover, the well-known cut-off law [20] predicts that the cut-off energy of an HHG spectrum equals $I_p + 3.17\, U_p$, with I_p the ionization potential of the gas and U_p the ponderomotive energy of the IR pulse. In these conditions, the cut-off energy is equal to 132 eV, the GDD of φ_{source} in the plateau region equals $3600\, as^2.rad^{-1}$, and becomes zero in the cut-off region [21]. Moreover, when plotted in logarithm scale, experimental spectra often appear to decrease linearly in the plateau region [6, 10], and to rapidly fall down in the cut-off region. Thus, we used this simplified shape for $S_{source}(\omega)$ (inset of figure 1 (b) as a basis for the optimization. Using equation (1), we deduced that the attosecond pulses $I_{source}(t)$ obtained in these conditions have a duration equal to 132 as and a typical profile [6] composed of a main peak followed by rapidly decreasing

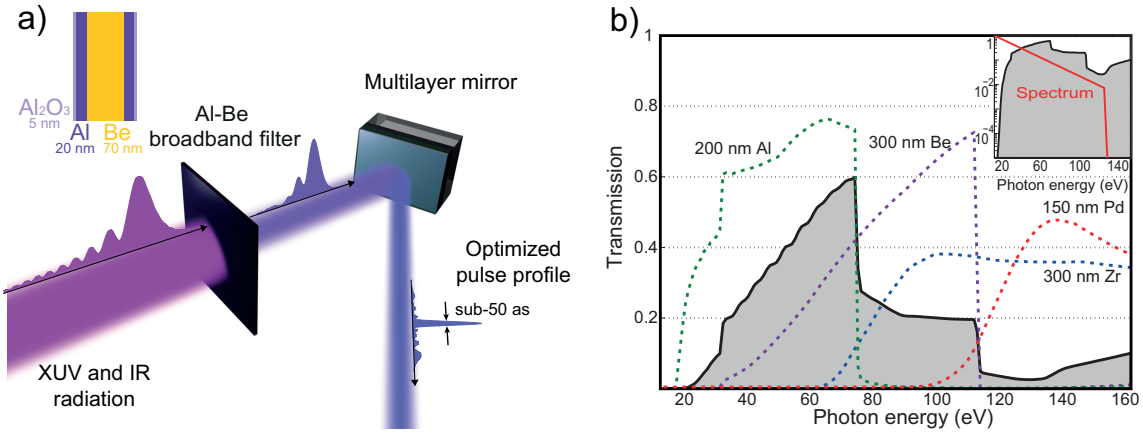

Figure 1. Temporal optimization of multilayer mirrors to obtain sub-50 as pulses. a) Principle of the temporal optimization. Inset: Structure of the hybrid filter. b) Transmission (gray shaded curve) of the Al-Be filter chosen for the design of the mirror, along with the transmission of typical filters (dashed lines), namely a 200 nm aluminum filter [13], a 300 nm beryllium filter [14], a 300 nm zirconium filter [15], and a 150 nm palladium filter [11]. Transmissions are calculated using the CXRO data base above 30 eV. Below, the Palick indices are used. This explains the imperfect connection of the transmission of the Al filter at 30 eV. Inset: The transmission of the Al-Be filter and the normalized XUV spectrum (red curve) are plotted in logarithm scale. The change of slope on the spectrum stands for the cut-off region.

bounces, see figure 2 (a).

$$I_{source}(t) = \left| \int_{-\infty}^{+\infty} S_{source}(\omega)^{1/2} \exp\left(i\varphi_{source}(\omega)\right) \cdot \exp(i\omega t)\, d\omega \right|^2 \qquad (1)$$

$$= \left| FT\left[S_{source}^{1/2} \cdot \exp\left(i\varphi_{source}\right) \right] \right|^2$$

2.2. The filter

The filter is a key component since it isolates the wanted spectral range from the rest of the spectrum. Especially, by absorbing lower energies, it allows one to suppress the IR beam used for the generation of the XUV radiation. Furthermore, the characterization of an attosecond pulse is usually based on the measurement of photoelectron spectra coming from the ionization of a rare gas by the XUV pulse [3, 4]. As a consequence, only photons carrying an energy greater than the ionization potential of the gas, say 15.76 eV in argon, will be represented in the electron spectra. Thus the use of a filter allows one to select a spectral range detectable in typical attosecond experiments.

Based on these considerations, we first considered typical filters, as depicted in figure 1 (b). As is well-known, the larger the spectrum, the shorter the Fourier-limited pulse. But it rapidly appeared that none of these filters had a bandwidth large enough

to attain sub-50 as durations with the chosen spectrum. Nevertheless, if combining together the $17-73\,eV$ bandwidth of an aluminum filter with the $40-112\,eV$ bandpass of a beryllium filter, one can select a very large range. However, adding the two independent filters in the beam will transmit the radiation only in the range where the two bandwidths overlap. But if their thicknesses are weak enough, one can get a significant transmission on the complete bandwidth. Consequently, we combined in a single filter a $70\,nm$ thick Be filter with a $40\,nm$ thick Al filter. Since the obtained hybrid filter is only made of a few layers and is used in transmission, the interferential effects in the stack are negligible. So the complex spectral response of the filter t_{filter} is equivalent to the product of the Al and Be filters taken independently. In order to ensure that the spectral response will be the same in the two possible ways of the filter, we made it symmetrical by encapsulating the $70\,nm$ thick Be layer between two $20\,nm$ Al layers. We also added two $5\,nm$ aluminum oxides Al_2O_3 layers on each side of the filter as in a realistic case, see the inset of figure 1 (a). Thus, the chosen filter has a total thickness greater than $100\,nm$ and is easily manufacturable [22]. Figure 1 (b) shows that its transmission simulated using the CXRO and Palick indices is comparable to other typical filters over the $17-112\,eV$ range. Moreover, its transmission falls down below $17\,eV$, as depicted in the inset of figure 1 (b), and equals 1.9×10^{-5} and 2.5×10^{-7} at $800\,nm$ and $11\,eV$ respectively. This ensures a good rejection of the IR beam and of the lowest energies. Finally, figure 2 (b) shows that the pulse $I_{in}(t)$ (see equation (2)) transmitted by the filter is $103\,as$ long, whereas the duration of the source pulse was equal to $132\,as$. This compression comes likely from the natural dispersion of aluminum and berrylium, which slightly compensates for the atto-chirp. Moreover, the duration of the Fourier limited pulse obtainable after the filter equals $47\,as$, which means that the bandpass of the filter is large enough to get sub-50 as pulses. However, these durations could be attained only if the phase dispersion is compensated by a properly designed multilayer mirror.

$$I_{in}(t)=\left|FT\left[S_{source}^{1/2}\cdot\exp\left(i\varphi_{source}\right)\cdot t_{filter}\right]\right|^2=\left|FT\left[S_{in}^{1/2}\cdot\exp\left(i\varphi_{in}\right)\right]\right|^2 \quad (2)$$

2.3. The multilayer mirrors

Multilayer mirrors for the XUV range are typically based on a periodic stack of molybdenum (Mo) and silicon (Si) layers. But being given that the radiation incoming on the mirror has complex spectral properties, the mirror spectral response optimizing the pulse shape and duration is not intuitive. Consequently, the best multilayer stack could be arbitrarily complex, that is to say not necessarily periodic. Thus we decided to optimize totally aperiodic structures. Moreover, in order to increase the reflectivity at low energy [23] and to minimize the interdiffusion of layers, we added a boron carbide (B_4C) layer between each Si and Mo layers. So the structure is composed of Mo-B_4C-Si-B_4C elementary stacks repeated several times. Due to the significant absorption of these materials in the selected spectral range, we expected that the total number of

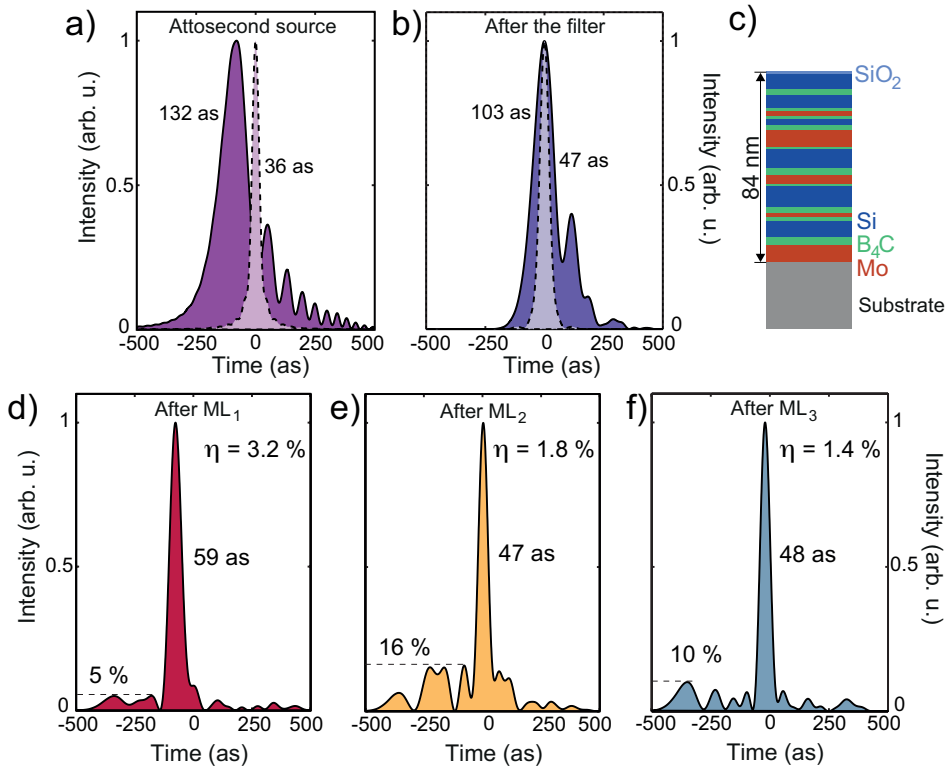

Figure 2. Theoretical pulse profiles before (a) and after (b) the filter, and after (d-f) reflection off one of the three multilayer mirrors optimized in the time-domain. a) (resp. b) Pulse profiles (continuous line) generated by the attosecond source (resp. transmitted by the filter) and the associated Fourier Transform limited pulse (dashed line). For a), the spectrum below the $17\,eV$ has been put to zero to compare the pulses before and after the filter on the same spectral range. c) Multilayer structure of the mirror ML_1. (d-f) Final pulse profile after the reflection off ML_1, ML_2 and ML_3, respectively. For each case, the FWHM duration, the relative fluence η, and the normalized intensity of the secondary peak are reported.

layers should not exceed a few tens of layers. Since the materials and the order of the layers were already chosen, the optimization process consisted only in finding their thicknesses. However, in order to obtain realistic multilayer stacks, we imposed the minimal thickness of a layer to be $0.8\,nm$. Finally, we added on top of the stack a $2\,nm$ thick Si layer, to allow the phase measurement (see section 4.), and a $1\,nm$ thick SiO_2 layer to take into account the unavoidable oxidation process. We chose an interfacial roughness equal to $0.3\,nm$ in the entire stack, which is usually obtained in our deposition machine. The last parameter to consider was the angle of incidence of the XUV beam on the structure. Due to the total reflection phenomenon occurring for grazing angles, the larger the incidence angle, the greater the reflectivity, but the less comprehensive the control of the phase of the mirror. Thus, we made a trade-off and chose to optimize the multilayer structures for a 22.5° incidence angle.

2.4. The temporal optimization algorithm

The optimization procedure of the thicknesses was based on a usual simulated annealing algorithm [24]. During the numerical process, the algorithm calculated the complex reflectivity of the multilayer $r_{mir}(\omega)$ as a function of the photon energy $\hbar\omega$. Then, knowing r_{mir} and the incoming spectrum S_{in} and spectral phase φ_{in}, the algorithm calculated the electric field of the reflected pulse $I_{out}(t)$ using equation (3):

$$I_{out}(t) = \left|FT\left[S_{in}^{1/2} \cdot \exp(i\varphi_{in}) \cdot r_{mir}\right]\right|^2 = \left|FT\left[S_{out}^{1/2} \cdot \exp(i\varphi_{out})\right]\right|^2 \quad (3)$$

As it is the case for every optimization algorithm, the simulated annealing finds the solution by minimizing an objective function. For the time-domain optimization, it had to take into account the relevant parameters of the wanted pulse. We chose to optimize the full-width at half maximum (FWHM) duration τ, which is the duration systematically given when measuring an isolated attosecond pulse [4, 15, 25] or an attosecond pulse train [3, 14]. However, the FWHM only describes the width of the main peak in the pulse profile, and ignores the rest of the pulse. Thus, we minimized the relative highness I_{2nd} of the second highest peak in the pulse profile in order to only get a main burst in the envelope. Finally, to make sure that the optimized pulses would carry a reasonably high energy, we chose the normalized fluence η (see equation (4)) of the pulse as the third parameter of the merit function, as shown in equation (5):

$$\eta = \int S_{out}(\omega)\, d\omega \Big/ \int S_{in}(\omega)\, d\omega \quad (4)$$

$$OF = w_\tau \cdot (\tau - \tau_{target})^2 + w_{I_{2nd}} \cdot (I_{2nd} - I_{2nd}^{target})^2 + w_\eta \cdot (\eta - \eta_{target})^2 \quad (5)$$

Where the X_{target} indicates the value targeted for the parameter X during the optimization, and w_X is the corresponding weight of the parameter X.

3. Optimization results and robustness

3.1. Results

We optimized three multilayer structures referred to as $ML_{1,2,3}$. The stacks are made of about twenty layers, the structure of the mirror ML_1 being reported on figure 2 (c) as a typical case. The pulse profiles obtained after reflection off each mirror are depicted in figure 2 (d-f). It appears that they are all composed of a main peak carrying the major part of the energy in the middle of a weakly intense $1\,fs$ temporal pedestal. This typical pulse shape is a direct consequence of the set of parameters chosen for the objective function, since neither τ, nor η, nor I_{2nd} is able to limit the temporal extension of this pedestal. Moreover, the relative fluence of the optimized pulses is greater than 1% in the three cases, which remains high enough to perform a pulse characterization [15].

Regarding the pulse duration and the second peak intensity, two approaches were chosen. In the case of ML_1, we imposed that I_{2nd} had to be as low as possible, and

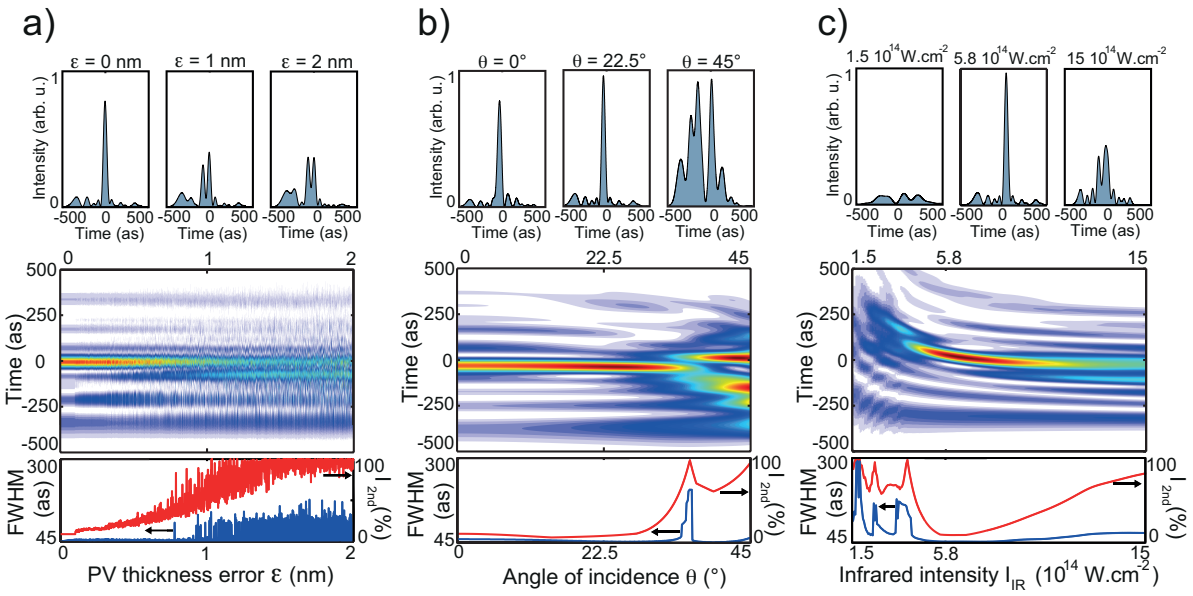

Figure 3. Evolution of the pulse profile after reflection off ML_3 with respect to environmental parameters. a) The PV thickness error of the deposited layers, b) the angle of incidence of the XUV beam on the mirror, and c) the intensity of the IR source generating the attosecond pulses were chosen as variable parameters. In each case, the continuous pulse evolution with respect to the chosen parameter is depicted (central panel), the pulse profile being detailed for three values of the parameter (upper panels). The evolution of the FWHM and the intensity of the secondary peak I_{2nd} (lower panels) is also depicted.

relaxed the condition on the FWHM which had to be lower than 60 as. Concerning ML_2 and ML_3, the trade-off was made on the second peak intensity which had to be lower than 20%. The targeted FWHM was the duration of the Fourier limited pulse after the filter (see the dashed line on figure 2 (b)), namely 47 as. We see on figure 2 (e-f) that the latter duration was attained for both mirrors and that I_{2nd} is equal to 16% and 10% for ML_2 and ML_3 respectively. Finally, if comparing the pulse generated by the source and the three pulse profiles obtained after the mirrors, we see that the FWHM has been divided by almost three.

3.2. Robustness to environmental conditions

However, these theoretical pulse profiles were optimized assuming given initial conditions, such as the shape of the initial XUV spectrum, or the angle of incidence of the pulse on the mirror. To make sure that the obtained mirrors will perform a pulse compression even though the environmental conditions slightly change, we simulated the evolution of the pulse profiles with respect to three parameters. The robustness of the three mirrors evolving the same way, we represented only ML_3 in order not to overload figure 3. First of all, in order to take into account the impact of a realistic fabrication process of the mirrors, we considered a deviation of the thicknesses of the

deposited layers from the expected ones. To be more specific, we randomly changed the thicknesses of each layer of the targeted multilayer structure of ML_3, the amplitude of the perturbation being given by the peak-to-valley (PV) thickness variation ϵ. In order to get a reliable tendency, we randomly drew 100 sets of thicknesses for each value of ϵ. Among the 100 obtained pulses, we plotted the one with the worst τ and I_{2nd} values in the upper and central parts of figure 3 (a), and we calculated the mean of τ and I_{2nd}, (see the lower panel of figure 3 (a)). The results highlight that ϵ should not exceed a few angströms in order to get the wanted pulse profile. Hopefully, the typical precision of our deposition machine is close to $0.3\,nm$ PV on the thickness of each individual layer, which lies in this tolerance range.

As a second parameter, we considered the incidence angle of the XUV beam on the mirror. The mirrors being optimized for an angle of 22.5°, we plot in figure 3 (b) the evolution of the pulse profile on the $[0°; 45°]$ range. The simulations show that the tolerance range of the mirror is remarkably large. Indeed, a compression of the pulse below $55\,as$ can be achieved in normal incidence as well as for a 30° incidence angle while keeping I_{2nd} below 20%. Moreover, the compression becomes optimal between 17.5° and 25°, the duration being below $50\,as$ and I_{2nd} being lower than 15%. Above 30°, the total reflection phenomenon becomes problematic. Indeed, the grazer the beam, the less it penetrates in the multilayer structure, the less effective the shaping of the pulse. Such a range of possible angles of incidence makes a pulse compression possible in various experimental setups.

The last variable parameter was chosen to be the intensity of the IR beam generating the XUV pulses. This quantity determines the cut-off energy of the HHG process, *i. e.* the extension of the XUV spectrum, and the value of the GDD responsible for the atto-chirp [6]. To explore a wide range around the initial intensity equal to $5.8\times10^{14}\,W.cm^{-2}$, we changed I_{IR} from $1.5\times10^{14}\,W.cm^{-2}$ to $15\times10^{14}\,W.cm^{-2}$. Consequently, the cut-off energy shifted from $50\,eV$ to $306\,eV$, and the GDD decreased from $14000\,as^2.rad^{-1}$ down to $1400\,as^2.rad^{-1}$. According to the simulations, the optimal range goes from $5\times10^{14}\,W.cm^{-2}$ to $8.5\times10^{14}\,W.cm^{-2}$. In these conditions, the FWHM remains below $50\,as$ and I_{2nd} does not exceed 20%. In an experimental set up, the typical precision when setting the IR intensity is much better than $1\times10^{14}\,W.cm^{-2}$ [6], so it is reasonable to think that one can easily work in the optimal range of compression.

These simulations showed that the pulse compression was possible in realistic experimental conditions. Consequently, the optimized multilayer structures were relevant and could be manufactured.

4. Fabrication and characterization of the mirrors

4.1. Fabrication

The multilayer stacks were deposited using a magnetron sputtering machine equipped with four cathodes [23]. Successive layers were deposited by scanning the substrate

above the target at a distance of $10\,cm$. During the process, we used a $0.27\,Pa$ argon pressure in the deposition chamber. The plasma discharges was established with a RF power of $150\,W$ for B_4C and Si targets and a DC current of $0.06\,A$ for the Mo target. The multilayer structure was controlled by means of a grazing-incidence Cu-$K\alpha$ reflectometer. Finally, the experimental performances of the deposited mirrors have been measured at the wavelengths of interest on a synchrotron beamline.

4.2. Principle of the characterization

Being given that the incident spectrum is very broad, the mirrors spectral response had to be characterized over a very large spectral range, namely from the cut-on of the Al-Be filter at $17\,eV$ up to the cut-off energy of the initial spectrum at $132\,eV$. In this range, the complete characterization of the mirrors implied to have an access both to the squared modulus R_{mir} and the phase φ_{mir} of the complex reflectivity r_{mir}. If the measurement of R_{mir} is now common, the determination of the phase is not straightforward. However, a possible method is based on the measurement of the Total Electron Yield, *i. e.* the current coming from the sample irradiated with synchrotron monochromatic light. In first approximation, this current is proportional to the standing wave coming from the interference between the amplitudes of the incident beam $A_{in}(\omega)$ and of the reflected beam $A_{out}(\omega)$ on top of the stack [19, 26]. In S polarization, the measured photocurrent $i_{mir}(\omega)$ is given by equation (6):

$$\begin{aligned} i_{mir}(\omega) &= C(\omega) \cdot |A_{in}(\omega) + A_{out}(\omega)|^2 \\ &= C(\omega) \cdot |A_{in}|^2 \cdot \left[1 + R_{mir} + 2R_{mir}^{1/2} \cdot \cos(\varphi_{mir})\right] \end{aligned} \tag{6}$$

In this equation, $C(\omega)$ is a parameter depending on the material from which the electrons are emitted, *i. e.* the material of the surface layer. To overcome this unknown, one needs to measure a reference photocurrent $i_{ref}(\omega)$. The latter has to come from a reference sample identical to the top layer of the multilayer stack, and for which $C(\omega)$ is supposed to be the same. Since the surface layer of the ML mirrors was chosen to be a silicon layer, the reference sample had to be composed of a simple silicon layer. Thus, if evaluating $J(\omega)$ corresponding to the ratio $\frac{i_{mir}(\omega)}{i_{ref}(\omega)}$, one can remove the influence of $C(\omega)$ as shown by equation (7).

$$J(\omega) = \frac{i_{mir}(\omega)}{i_{ref}(\omega)} = \frac{1 + R_{mir} + 2R_{mir}^{1/2} \cdot \cos(\varphi_{mir})}{1 + R_{ref} + 2R_{ref}^{1/2} \cdot \cos(\varphi_{ref})} \tag{7}$$

But, if the reflectivities of the mirror $R_{mir}(\omega)$ and of the reference sample $R_{ref}(\omega)$ are easily measurable, the reference phase $\varphi_{ref}(\omega)$ remains unknown. However, if rearranging equation (7) into equation (8), one can notice that the lower the ratio $\sqrt{\frac{R_{ref}}{R_{mir}}}$, hereafter referred to as ρ, the less significant the role of φ_{ref} in the reconstructed phase φ_{mir}.

$$\cos(\varphi_{mir}(\omega)) = J \cdot \left[\frac{1 + R_{ref}}{2R_{mir}^{1/2}} + \rho \cdot \cos(\varphi_{ref})\right] - \frac{1 + R_{mir}}{2R_{mir}^{1/2}} \tag{8}$$

Moreover, $\cos(\varphi_{ref})$ being always included in the $[-1;1]$ interval, one can limit $\cos(\varphi_{mir})$ by two functions $L_{\pm}$ using inequality (9). Consequently, measuring $J(\omega)$, $R_{mir}(\omega)$ and $R_{ref}(\omega)$ allows one to reconstruct the phase of the multilayer mirror with an accuracy depending on the quantity ρ.

$$L_{-}(\omega) \leq \cos(\varphi_{mir}(\omega)) \leq L_{+}(\omega) \tag{9}$$

Where $L_{\pm}$ equals $\left[J\left(1+R_{ref} \pm 2R_{ref}^{1/2}\right) - 1 + R_{mir}\right] \cdot \left(2R_{mir}^{1/2}\right)^{-1}$.

4.3. Results of the characterization

According to the previous analysis, the photoelectrons are supposed to come only from the surface of the measured material. Consequently, $i_{ref}(\omega)$ should not depend on the thickness of the silicon reference sample. To verify this hypothesis, we manufactured a $10\,nm$ thick and a $20\,nm$ thick silicon reference sample, and measured their reflectivities and photocurrents on the BEAR beamline on the Elettra synchrotron, see figure 4 (a) and (b). As expected, the photocurrents of the two reference samples are extremely similar. As for their reflectivities, they are very low in both cases, and are modulated with an oscillation, the period of which is determined by the thickness of the silicon layer. After the fine characterization of the reference samples, it was possible to use them to extract the phase of the ML mirrors.

Consequently, we measured the reflectivity and the photocurrent of the three mirrors, and used the phase extraction process previously described. The reference phase φ_{ref} being unknown, we plotted in the case of ML_1 the range of the possible $\cos(\varphi_{mir})$ using equation (9), as depicted in figure 4 (c). When ρ is low, roughly on the $40-100\,eV$ spectral range, the shaded area delimited by L_{-} and L_{+} strongly narrows, allowing one to estimate the phase of the mirror with a good precision. Moreover, due to the modulations in the reflectivities of the reference samples, R_{ref} and thus ρ become periodically very low. On the opposite, for the lowest and highest energies, R_{ref} becomes of the same order of magnitude than R_{mir}, see figure 4 (a). Consequently, ρ becomes significant leading to a bad accuracy of the phase measurement. Applying the arccos function to the data in figure 4 (c) allowed one to get the phase φ_{mir} of the mirror. The reconstructed phase had then to be unwrapped by changing its sign and by adding a π offset every time the phase reaches 0 or π. Finally, the two experimental unwrapped phases reconstructed from the two reference samples were averaged, the final phase being depicted on figure 5 (d-f) for the three mirrors along with their reflectivities in figure 5 (a-c).

Concerning ML_1 and ML_2, the agreement between the experimental phase and the simulated one is very good, the latter being almost always included in the shaded area. Moreover, the global tendency of the phase as well as its most rapid variations are well reproduced in the $40-100\,eV$ range. The same agreement can be observed for their reflectivity too, except around $40\,eV$, as shown in figure 5 (a) and (b). This is most likely due to a deviation of the actual indices of refraction in this range from the tabulated

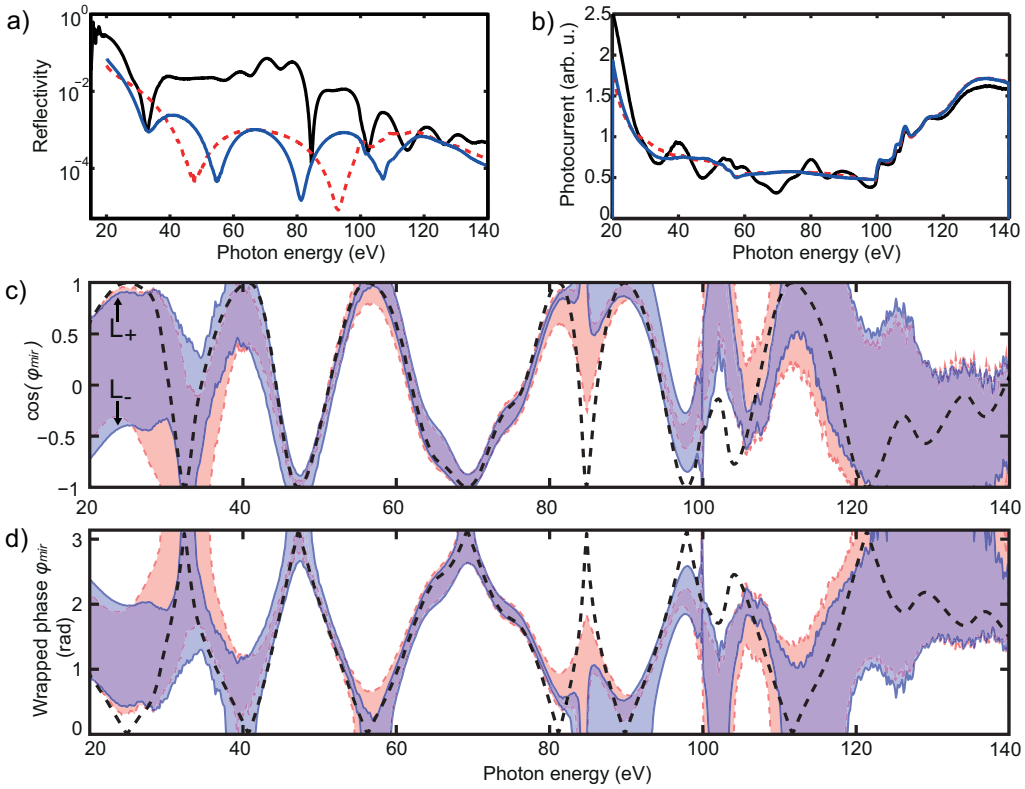

Figure 4. Principle of the extraction of the phase of the mirror from reflectivity and photocurrent measurements. a) Reflectivity and b) photocurrent of ML_1 (black curve), and the $10\,nm$ (red dashed curve) and $20\,nm$ (blue continuous curve) reference samples. c) Evolution of the experimental $L_{\pm}(\omega)$ functions (shaded curves) delimiting the range of the possible $\cos(\varphi_{mir})$ of ML_1 obtained with the $10\,nm$ (red dashed line) and the $20\,nm$ (blue continuous line) reference samples. d) Range of the possible phase of the mirror φ_{mir} (blue and red shaded curves) reconstructed from the data in c). In (c-d), the black dashed line represents the cosine of the simulated phase and the wrapped simulated phase respectively.

ones used for the optimization. Regarding ML_3, the agreement appears to be less good. If the global shape of the reflectivity is more or less respected, the two main spikes around $80\,eV$ are clearly shifted of a few electron-volts with respect to the simulated reflectivity. Moreover, the same shift affects the cosine of the phase extracted from the photocurrents measurements, see the inset in figure 5 (f), and the unwrapped phase. After studying the multilayer mirror by the use of a Cu-Kα reflectometer, it appears that this shift comes from the formation of a new chemical compound at each interface between a B4C layer and a Mo layer, when these two layers are too thin.

Finally, it should be noticed that the simulated and measured spectral responses of

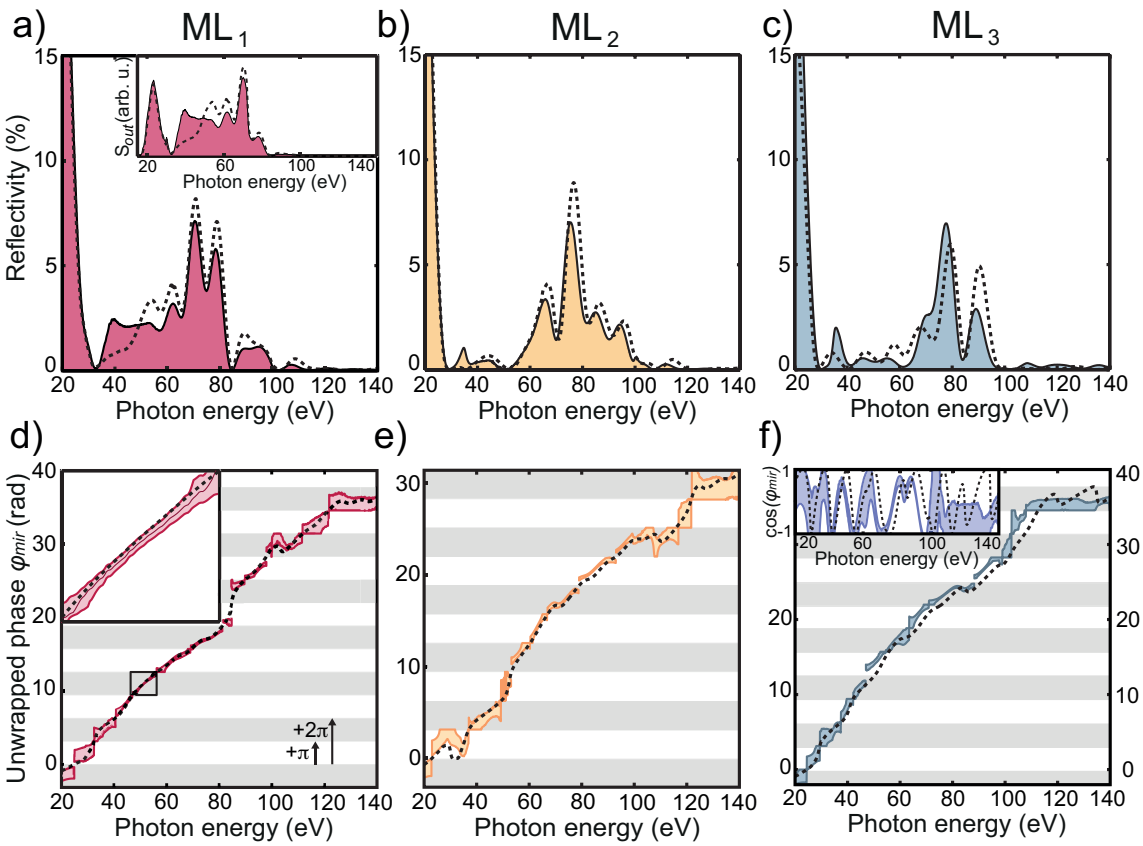

Figure 5. Characterization of the reflectivity (a-c) and the phase (d-f) of the three multilayer mirrors. The simulated reflectivities and phases (dashed lines) are depicted along with the measurements (shaded lines). In a), the inset represents the spectrum $S_{out}(\omega)$ reflected off the mirror ML_1 deduced from S_{in} and the measured (shaded line) and simulated (dashed line) reflectivities. The inset in d) corresponds to a zoom in on the spectral range $47-56\,eV$. The continuous line in the shaded area corresponds to the phase reconstructed if assuming that $\cos(\varphi_{ref})$ equals zero. In f), the inset represents the simulated $\cos(\varphi_{mir})$ (dashed line) and the one reconstructed from the $20\,nm$ reference sample (blue shaded area). In (a-c), the simulated reflectivities take into account the $(80;20)$ polarization of the synchrotron beamline. In (d-f), the gray and white strips stand for the π offsets added to unwrap the experimental phases.

these mirrors are not intuitive. Until now, when designing mirrors for the compression of attosecond pulses, most of the targeted phase behaviors were a constant and negative GDD, that is to say a convex parabolic phase profile [9, 10, 11, 19, 26]. With the temporal optimization, the obtained phase profiles are not parabolic anymore. More precisely, the phases of the three mirrors clearly tend to be convex, but they are modulated by fluctuations around this global curvature. However, the latter do not prevent from obtaining an effective compression, the duration of the final pulse being guaranteed by the time domain optimization. This observation has already been made for chirped dielectric mirrors for the compression of IR femtosecond pulses [16], and appears to be

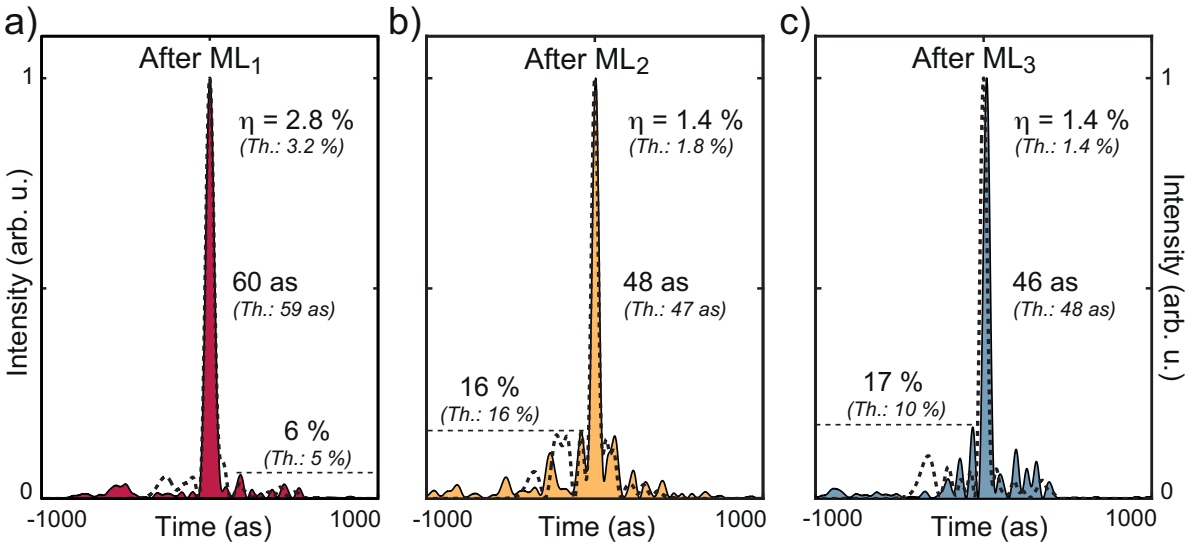

Figure 6. Reconstructed pulse profiles based on the measured mirrors properties. (a-c) The shaded lines correspond to the pulse profiles deduced from the measured reflectivities and from the phases obtained if assuming $\cos(\varphi_{ref})$ equal to 0. The theoretical profiles (dashed line) are also represented. In each case, the duration FWHM, the second peak intensity and the normalized fluence η are depicted along with the theoretical values.

relevant for the compression of attosecond pulses too.

In order to completely characterise the mirrors, the ultimate step is to reconstruct the reflected pulses from the experimental responses of the mirrors. To do so, one needs to consider a given phase evolution in the range of the possible phases, *i. e.* to choose a curve in the shaded area in figure 5 (d-f). Thus, we chose the case where $\cos(\varphi_{ref})$ equals zero as an average case, see the inset of figure 5 (d). The resulting pulse profiles are depicted in figure 6. In the three cases, the reconstructed pulses are very close to the expected ones. Especially, the durations obtained after ML_2 and ML_3 are below $50\,as$ while keeping the second peak below 20 %.

After reflection off one of the mirrors, the attosecond pulses become single-cycle, as shown on figure 7. In an experiment involving such pulses, the response of the medium interacting with the pulse will not be averaged over many optical cycles. The medium will rather interact directly with the electric field of the pulse. And this interaction will strongly depend on the carrier-envelope phase (CEP) of the pulses, that is the phase-shift between the centre of the pulse and the maximum of the electric field. Moreover, a theoretical study [25] highlighted that the CEP of attosecond pulses was robust to reasonable variations of the generation conditions. Consequently, attosecond pulses could be generated without significant shot to shot variations of their CEP state. However, if a post-compression of these attosecond pulses is performed with multilayer mirrors, a modification of their CEP can be induced during the reflection off the mirror. Thus, it becomes important to estimate experimentally the impact on the attosecond

CEP. Furthermore, the carrier-envelope phase cannot be measured by current attosecond pulse characterization techniques, such as the RABITT technique [3, 6, 10] or the CRAB technique [11, 27]. Indeed, these methods reconstruct the pulse spectral phase up to a constant, the information about the CEP being encoded in this very constant. However, the modification of the CEP induced by the mirror is accessible through the photocurrents technique, since the latter allows one to reconstruct the absolute spectral phase of the mirror. Consequently, we made a study based on the experimental results to estimate the variation of the CEP after the reflection off the mirrors.

5. Control of the Carrier-Envelope Phase of attosecond pulses

Rigorously, one can define the CEP φ_{CE} of a pulse as the opposite of the temporal phase $\phi(t)$ taken at the arrival time t_0 of the pulse, that is when the maximum intensity is reached :

$$\varphi_{CE} = -\phi(t_0) \tag{10}$$

Thus the first step when determining the CEP of a pulse is to identify its arrival time t_0.

5.1. Time spent by the pulse in the multilayer stack

Consider a fictitious detector placed at a given position along the pulse propagation axis. One can define the arrival time t_0 of the pulse as the moment when the pulse reaches its maximum intensity on the detector. If putting a multilayer mirror on the way, the variation of the arrival time Δt_0 will correspond to the time that the pulse spent in the multilayer structure, see figure 7. As shown in figure 7 (a), the duration of the reflection measured in the case of ML_1 equals $245 \pm 3\,as$, which is very close to its theoretical value of $243\,as$. Regarding the other mirrors, the pulse should spend more time in the multilayer stack since Δt_0 was estimated to be equal to $327 \pm 2\,as$ and to $317 \pm 4\,as$ for ML_2 and ML_3 respectively.

5.2. Carrier-Envelope Phase offset induced by the mirror

But the reflection of the attosecond pulse on a mirror can also induce a change of its CEP. This phase shift $\Delta\varphi_{CE}$ can be evaluated on figure 7. Indeed, in this figure, the CEP of the incident pulse was chosen to be zero, so that estimating the CEP of the reflected pulse is equivalent to measuring $\Delta\varphi_{CE}$. Especially, in the case of ML_1, the measured CEP shift is equal to $2.2 \pm 0.3\,rad$, the theoretical value being equal to $2.0\,rad$. As for ML_2 and ML_3, we estimated $\Delta\varphi_{CE}$ to be equal to $-2.2 \pm 0.1\,rad$ and to $-1.9 \pm 0.4\,rad$ respectively. This highlights some similarities in the behaviour of ML_2 and ML_3. Indeed, for these two mirrors, the duration of the reflection process is slightly longer than in the case of ML_1, and the CEP shift that they induce appears to be negative, as opposed to a positive shift for ML_1.

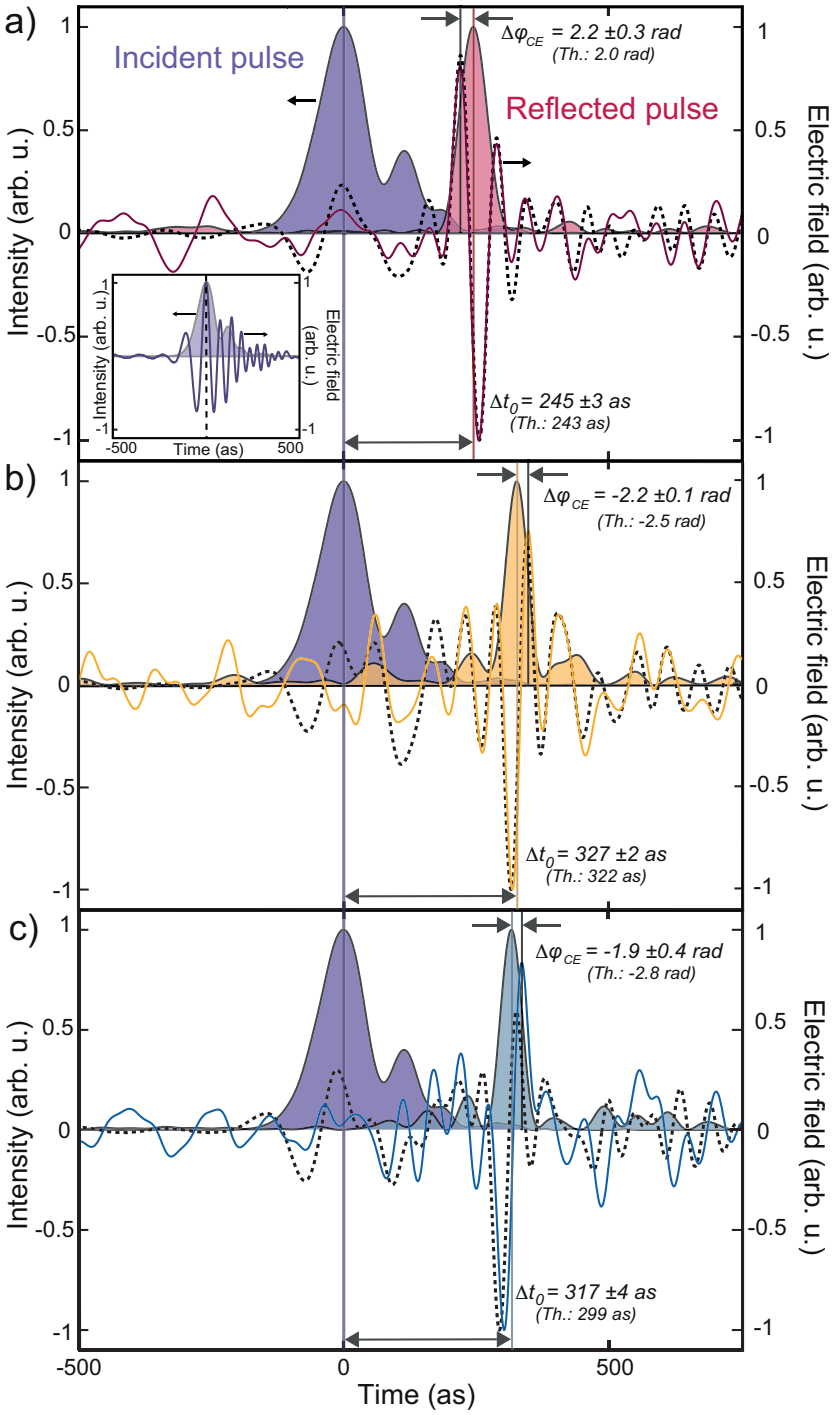

Figure 7. Experimental and theoretical influence of the mirrors on the reflected attosecond electric field. For ML_1 (a), ML_2 (b) and ML_3 (c), the incident pulse (purple shaded line) and the reconstructed reflected pulses (red, yellow and blue shaded lines) are represented. The continuous oscillating lines stand for the experimentally reconstructed electric field after reflection off the mirrors, the dashed lines corresponding to the simulated electric field. As shown in the inset in a), the CEP of the incident pulse was assumed to be 0. In each case, the experimental and theoretical values of the duration of the reflection of the pulse Δt_0, and of the CEP shift $\Delta\varphi_{CE}$ are depicted.

This measurement of the offset of the CEP due to the reflection on a mirror has to be seen as a proof of concept which will have to be improved. Moreover, even though the influence of the mirror on the CEP can be measured, it has not been taken into account in the optimization process. Thus we can imagine modifying the objective function to optimize a mirror compressing attosecond pulses and giving them a wanted CEP state.

6. Conclusion

By using the time domain approach, we optimized a broadband filter and three multilayer mirrors to compress attosecond pulses down to theoretical durations between $59\,as$ and $47\,as$ FWHM. Moreover, a theoretical study highlighted that the tolerance of the mirrors to the variations of the experimental conditions were good. In particular, the mirrors can ensure an efficient pulse compression in a very large range of angles of incidence. We then manufactured the mirrors and characterized them on a synchrotron beamline both in reflectivity and phase. Especially, the measurement of the latter was performed thanks to the photocurrent technique over a $120\,eV$ large spectral range. The very good overall agreement with simulated phases allowed us to estimate experimentally the time spent by an attosecond pulse in the multilayer mirrors during the reflection process. We also measured the impact of the mirrors on the attosecond carrier-enveloppe phase. This opens the route toward attosecond electric field shapers based on multilayer mirrors.

7. References

[1] McPherson A, Gibson G, Jara H, Johann U, Luk T S, McIntyre I A, Boyer K and Rhodes C K 1987 *J. Opt. Soc. Am. B* **4,** 595.

[2] Ferray M, L'Huillier A, Li X F, Lompre L A, Mainfray G and Manus C 1988 *J. Phys. B* **21,** L31.

[3] Paul P M, Toma E S, Breger P, Mullot G, Augé F, Balcou Ph, Muller H G and Agostini P 2001 *Science* **292,** 1689-1692.

[4] Hentschel M, Kienberger R, Spielmann Ch, Reider G A, Milosevic N, Brabec T, Corkum P, Heinzmann U, Drescher M and Krausz F 2001 *Nature* **414,** 509-513.

[5] Nomura Y *et al.* 2009 *Nature Phys.* **5,** 124-128.

[6] Mairesse Y*et al.* 2003 *Science* **302,** 1540.

[7] Kim K T, Kim C M, Baik M-G, Umesh G and Nam C H 2004 *Phys. Rev. A* **69,** 051805.

[8] Wonisch A, Westerwalbesloh T, Hachmann W, Kabachnik N, Kleineberg U and Heinzmann U 2004 *Thin Solid Films* **464-465,** 473.

[9] Morlens A-S, Balcou Ph, Zeitoun Ph, Valentin C, Laude V and Kazamias S 2005 *Opt. Lett.* **30,** 1554.

[10] Bourassin-Bouchet C *et al.* 2011 *Opt. Express* **19,** 3809-3817.

[11] Hofstetter M *et al.* 2011 *Opt. Express* **19,** 1767-1776.

[12] Poletto L, Frassetto F and Villoresi P 2008 *J. Opt. Soc. Am. B*, **25,** B133-B136.

[13] López-Martens R *et al.* 2005 *Phys. Rev. Lett.* **94,** 033001.

[14] Ko D H, Kim K T, Park J, Lee J and Nam C H 2010 *New J. Phys.* **12,** 063008.

[15] Goulielmakis E *et al.* 2008 *Science* **320,** 1614.

[16] Dombi P, Yakovlev V S, O'Keeffe K, Fuji T, Lezius M and Tempea G 2005 *Opt. Express* **13,** 10888-10894.

[17] Pervak V, Ahmad I, Fulop J, Trubetskov M K and Tikhonravov A V 2005 *Opt. Express* **17,** 2207-2217.
[18] Wonisch A, Neuhäusler U, Kabachnik N M, Uphues T, Uiberacker M, Yakovlev V, Krausz F, Drescher M, Kleineberg U and Heinzmann U 2006 *Appl. Opt.* **45,** 443.
[19] Aquila A, Salmassi F and Gullikson E 2008 *Opt. Lett.* **33,** 455.
[20] Corkum P B 1993 *Phys. Rev. Lett.* **71,** 1994-1997.
[21] Mairesse Y*et al.* 2004 *Phys. Rev. Lett.* **93,** 163901.
[22] Soufli R and Gullikson E 1998 *Appl. Opt.* **37,** 1713-1719.
[23] Gautier J, Delmotte F, Roulliay M, Bridou F, Ravet M-F and Jérome A 2005 *Appl. Opt.* **44,** 384.
[24] Kirkpatrick S, Gelatt C D, and Vecchi M P 1983 *Science* **220,** 671.
[25] G. Sansone *et al.* 2006 *Science* **314,** 443.
[26] Suman M, Monaco G, Pelizzo M-G, Windt D L and Nicolosi P 2009 *Opt. Express* **17,** 7922.
[27] Mairesse Y and Quéré F 2005 *Phys. Rev. A* **71,** 011401.